Article

# An Improved Organic Solar Cell Lumped-Parameter Equivalent Circuit Model

Chuanzhong Xu, Fei Yu, Wei Lin and Gongyi Huang

Special Issue

Selected Papers from Taiwan Association for Academic Innovation, TAAI 2018

Edited by
Prof. Dr. Chien-Jung Huang, Prof. Dr. Kuan Chee and Dr. Yeu-Long Jiang

# An Improved Organic Solar Cell Lumped-Parameter Equivalent Circuit Model

**Chuanzhong Xu †, Fei Yu \*,† [ID], Wei Lin and Gongyi Huang**

College of Information Science and Engineering, Huaqiao University, Xiamen 361021, China;
xucz@hqu.edu.cn (C.X.); linwei_0311@126.com (W.L.); hgy@hqu.edu.cn (G.H.)

\* Correspondence: yufei_jnu@126.com; Tel.: +86-0592-6162-385

† These two authors contributed equally to this work.

**Abstract:** An improved lumped-parameter equivalent circuit model is proposed to describe S-shaped *I–V* characteristics of organic solar cells (OSCs). This model originates but differs from Mazhari's model. As a minor but important modification, a shunt resistance is added to Mazhari's model to increase the accuracy of simulating the S-shaped kink in the third quadrant. Subsequently, we present a terminal current-voltage equation set and derive an analytical solution to the improved model. Furthermore, we verify the analytical solution to our model by using the least square method and validate our model by using the experimental *I–V* curves examined from OSCs. Compared with Mazhari's model, our model has greater accuracy in interpreting the S-shaped kink with linear-like rise in the third quadrant. As a result, our improved model is suitable to explain the S-shaped *I–V* characteristics of organic solar cells in the whole operational region, especially for the S-shaped kink in the third quadrant.

**Keywords:** lumped-parameter model; organic solar cells; equivalent circuit; S-shaped kink

## 1. Introduction

Over the last two decades, organic photovoltaic devices [1] have attracted much attention and undergone intensive research due to their many potential advantages over conventional silicon-based solar cells, such as low-cost printing [2] and fabrication on flexible substrate [3]. However, the power conversion efficiency (PCE) of organic solar cells (OSCs) still cannot approach that of conventional silicon-based solar cells because the S-shaped kinks that are tested according to the *I–V* characteristics of polymer OSCs [4,5] can damage the PCE. Recently, the bilayer cell structure based on heterojunction [6,7] has been reported to give a crucial improvement in PCE, but the efficiency so far is not high enough. It is noted that a lumped-parameter equivalent circuit model of OSCs is useful to explain three factors [8] impacting PCE—short-circuit current, open-circuit voltage, and fill factor—and to optimize the design of photovoltaic devices by providing a quantitative analysis for *I–V* characteristics.

The conventional equivalent circuit models [9,10] of Si-based solar cells obviously cannot reasonably interpret the S-shaped kink observed in OSCs, because the constant photo-generated current source, in parallel with a single diode, only represents the J-shaped *I–V* curves. Among the multiple-diode equivalent circuit models [11–17], Mazhari's model [11] is regarded as the simplest model including seven parameters used in simulations, while the other models [12–17] contain at least eight fitting parameters. Mazhari's model is able to provide an electrical explanation [18] of the OSC S-shaped kink with exponential-like rise in the first quadrant, but it fails to demonstrate the linear-like rise of the S-shaped kink of OSCs in the third quadrant [19].

In this paper, we propose an improved lumped-parameter equivalent circuit model by modifying Mazhari's model, in order to give accurate predictions on *I–V* characteristics of OSCs, especially for

the linear-like upturn in the S-shaped kink in the third quadrant. The rest of the paper is organized as follows. In Section 2, the set of *I–V* equations in the improved model is shown and the analytical solution is derived. In Section 3, we verify the solution by using the least square method results. In Section 4, we compare our model and Mazhari's model with experimental data [20], and discuss why our model is more accurate. Finally, the conclusions are summarized in Section 5.

## 2. Improved Model and Its Analytical Solution

As shown in Figure 1, Mazhari's model consists of three diodes (i.e., $D_D$, $D_R$, and $D_E$) and a photo-generated current source $I_{ph}$ without any series or shunt resistances. In the above-mentioned diodes, $D_D$ simulates the dark current, $D_R$ models the recombination current, and $D_E$ describes the extraction current. The absence of series or shunt resistances leads to the introduction of major errors in the process of simulating the S-shaped kink in the third quadrant.
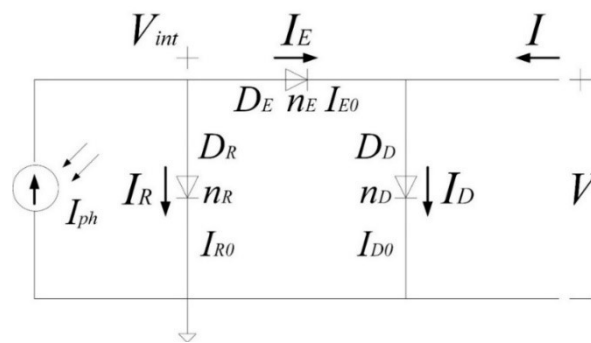


**Figure 1.** The solar cell lumped-parameter equivalent circuit model [11] proposed by Mazhari.

Based on Mazhari's model, we propose an improved model as shown in Figure 2. We add a shunt resistance with the diode $D_R$ to supply a linear item in the relationship between terminal current *I* and voltage *V* in Figure 2, which is beneficial for illustrating the S-shaped kink with linear-like rise in the third quadrant, as shown in Section 4. In addition, there are two things deserving of our attention. From the aspect of the circuit's topological structure, adding the shunt resistance $R_s$ with the diode $D_R$ in Figure 2 is equivalent to placing the resistance directly in series or in parallel with the photocurrent, according to the law of external equivalence. From the physical significance aspect, the shunt resistance $R_s$ with $D_R$ in Figure 2 represents the power conversion efficiency (PCE) loss resulting from the contact resistances between electrode and acceptor, between acceptor and donor, and between donor and electrode.
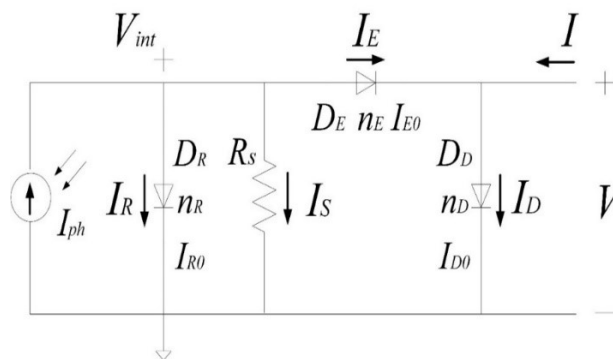


**Figure 2.** The improved solar cell lumped-parameter equivalent circuit model.

In Figure 2, at two earth-free nodes, we use Kirchhoff's current law and Shockley's well-known ideal diode current equation [21] to obtain two node current equations as

$$I_{ph} = I_E + I_R + I_S = I_{E0}\left(e^{\frac{V_{int}-V}{n_E V_t}} - 1\right) + I_{R0}\left(e^{\frac{V_{int}}{n_R V_t}} - 1\right) + \frac{V_{int}}{R_S}, \tag{1}$$

$$I = I_D - I_E = I_{D0}\left(e^{\frac{V}{n_D V_t}} - 1\right) - I_{E0}\left(e^{\frac{V_{int}-V}{n_E V_t}} - 1\right) \tag{2}$$

It is worth noting that Equation (2) can be directly applied to Figure 1, but the linear item introduced by the shunt resistance that $R_S$ is added into Equation (1) is different from that in Figure 1. Here, $V_{int}$ is the voltage drop across the recombination diode $D_R$. $n_D$, $n_R$, and $n_E$ are the ideality factors of three diodes representing the divergence from the ideal diode. $I_{D0}$, $I_{R0}$, and $I_{E0}$ are the reverse saturation currents of three diodes. $V_t$ is the thermal voltage symbolized by $kT/q$, where $k$ is the Boltzmann constant, $T$ is the absolute temperature, and $q$ is the electron charge.

Aiming at roundly demonstrating the S-shaped *I–V* characteristics of OSCs, implementing our improved model into OSCs' *I–V* characteristic simulations in compact format, and facilitating the computer-aided-design, we should derive the accurate and efficient solution of the equation set of Equations (1) and (2) to demonstrate the terminal current *I* as a function of the terminal voltage *V* in the improved model, i.e., *I–V* characteristics of OSCs. Unfortunately, the above equation set cannot be solved directly because Equations (1) and (2) are transcendental equations including at least two exponents. Although we can use the least square method to find the accurate solution of the equation set, this method actually consumes much more computation time, leading to reduced simulation efficiency.

In this paper, we pay more attention to Equation (1) rather than substituting Equation (1) into Equation (2) and eliminating $V_{int}$ to directly solve the implicit *I–V* equation. We use the Newton–Raphson root-finding scheme [19], as a trade-off method between accuracy and efficiency, to derive an analytical solution of Equation (1) obtaining the computation results of $V_{int}$ as a function of *V*. Subsequently, we substitute $V_{int}$ into Equation (2) to get the results of the *I–V* equation in Figure 2. It is noted that the Newton–Raphson root-finding scheme adopted in solving Equation (1) processes the fast convergence and enough computation accuracy.

## 3. Numerical Verification and Discussion

In this section, we use the least square method to verify the solution derived by the Newton-Raphson root-finding scheme of our improved model. In Figures 3–8, the verifications show that good agreements between our solutions and the least square method results can be obtained and our improved model can describe the S-shaped *I–V* characteristics of OSCs. Here, we can requisite the fitting parameters used in simulations by using the systematic parameter extraction procedure presented in Reference [11] or Reference [18].

Furthermore, we will now discuss the influences of the different fitting parameters on $V_{int}$ and *I*. Firstly, Figure 3 shows that $R_S$ has an effect on both $V_{int}$ and *I*. $R_S$ determines the slopes of $V_{int}$ (shown in Figure 3a) and *I* (shown in Figure 3b) as a function of *V* in the third quadrant, respectively. It is noted that $R_S$ has little effect on $V_{int}$ and *I* while $R_S$ is larger than 1 k$\Omega$. In fact, this is in consistent with the circuit structure in Figure 1. If $R_S$ comes into infinity, our improved model in Figure 2 would degrade into Mazhari's model in Figure 1. Secondly, Figure 4 shows that $I_{ph}$ can affect the quantities of $V_{int}$ in the whole operational region and *I* in the third quadrant, but not the slopes of $V_{int}$ and *I*. Thirdly, Figures 5 and 6 show that the recombination diode $D_R$ has an important influence on the characteristics of OSCs. On the one side, in Figure 5a, we can observe that $I_{R0}$ only affects the results of $V_{int}$ in the first quadrant. In Figure 5b, $I_{R0}$ affects the results of *I* only in the third quadrant. On the other side, in Figure 6a,b, the role played by $n_E$ is analogous to that of $I_{R0}$. On the contrary, $I_{E0}$ and $n_E$ of the extraction diode $D_E$ can only influence the results of $V_{int}$ in the first quadrant, but not in the third quadrant, as shown in Figures 7a and 8a. At the same time, both $I_{E0}$ and $n_E$ can only affect the results of *I* in the third quadrant, as shown in Figures 7b and 8b.
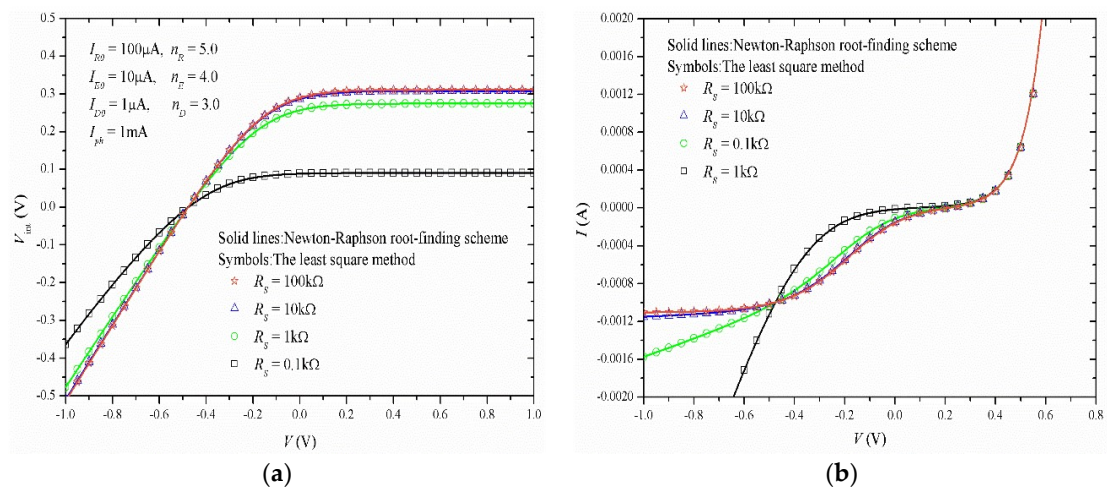
**Figure 3.** Electrostatic characteristics of organic solar cells (OSCs) simulated by our improved model for the different $R_S$. (**a**) $V$ vs. $V_{int}$; (**b**) $V$ vs. $I$.
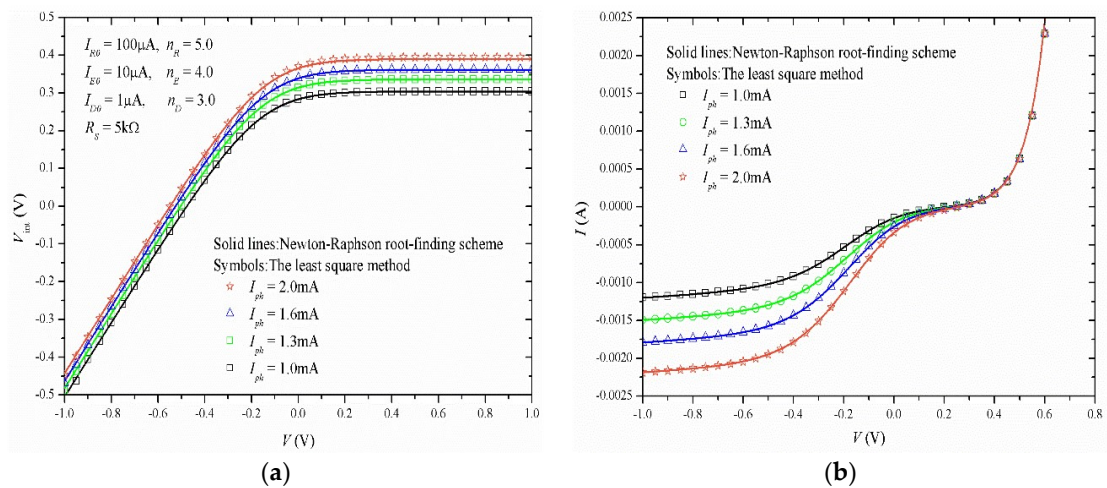


**Figure 4.** Electrostatic characteristics of OSCs simulated by our improved model for the different $I_{ph}$. (**a**) $V$ vs. $V_{int}$; (**b**) $V$ vs. $I$.
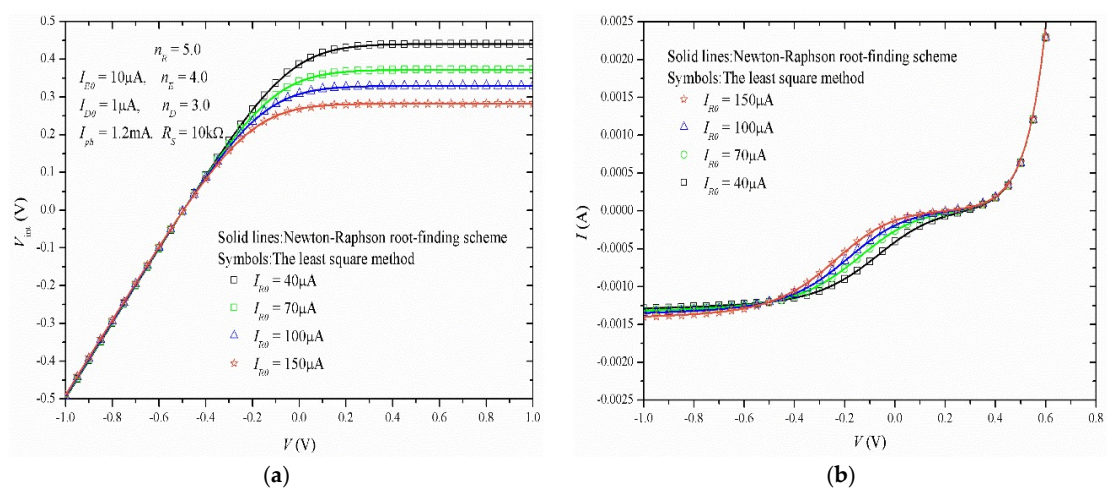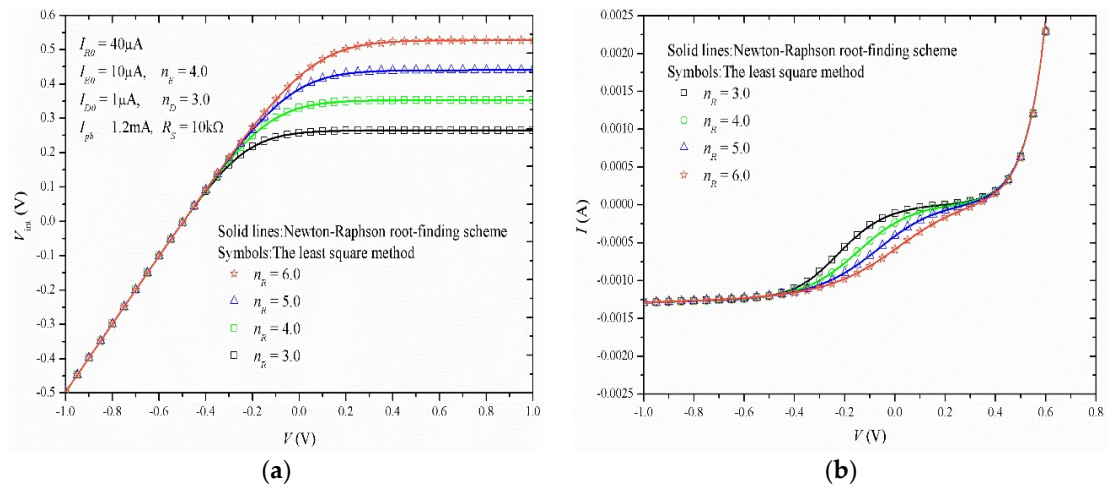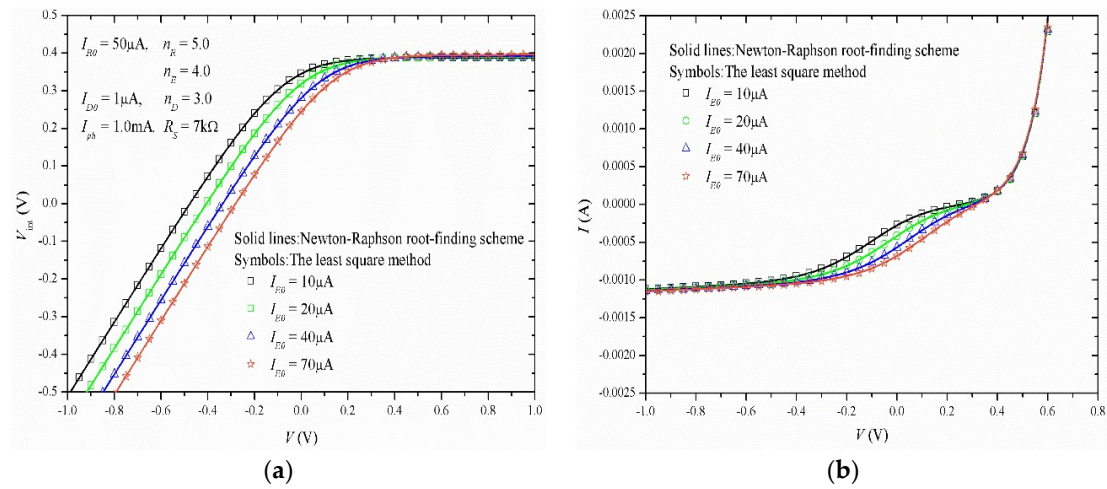


(**a**)　　　　　　　　　　　　　　　　　　　　　　　(**b**)

**Figure 5.** Electrostatic characteristics of OSCs simulated by our improved model for the different $I_{R0}$. (**a**) $V$ vs. $V_{int}$; (**b**) $V$ vs. $I$.
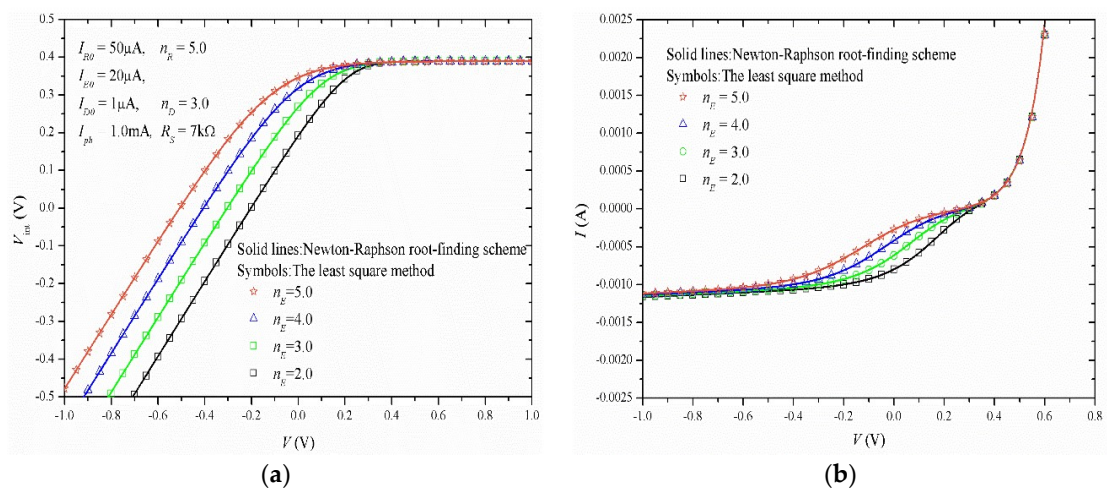
**Figure 6.** Electrostatic characteristics of OSCs simulated by our improved model for the different $n_R$. (**a**) $V$ vs. $V_{int}$; (**b**) $V$ vs. $I$.



**Figure 7.** Electrostatic characteristics of OSCs simulated by our improved model for the different $I_{E0}$. (**a**) $V$ vs. $V_{int}$; (**b**) $V$ vs. $I$.



**Figure 8.** Electrostatic characteristics of OSCs simulated by our improved model for the different $n_E$. (**a**) $V$ vs. $V_{int}$; (**b**) $V$ vs. $I$.

## 4. Experimental Verification and Comparison with Mazhari's Model

In Figures 9–13, we compare the solutions of our improved model with experimental data [19] to verify our model in practice. Simultaneously, the results simulated by Mazhari's model are shown in Figures 9–13, which may be compared with our improved model.
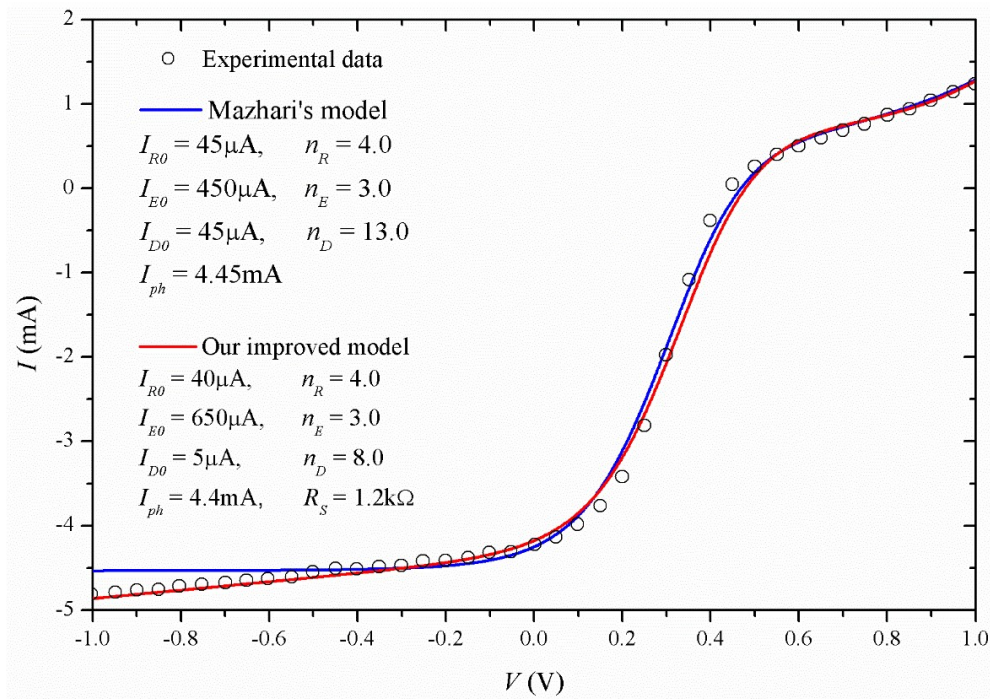


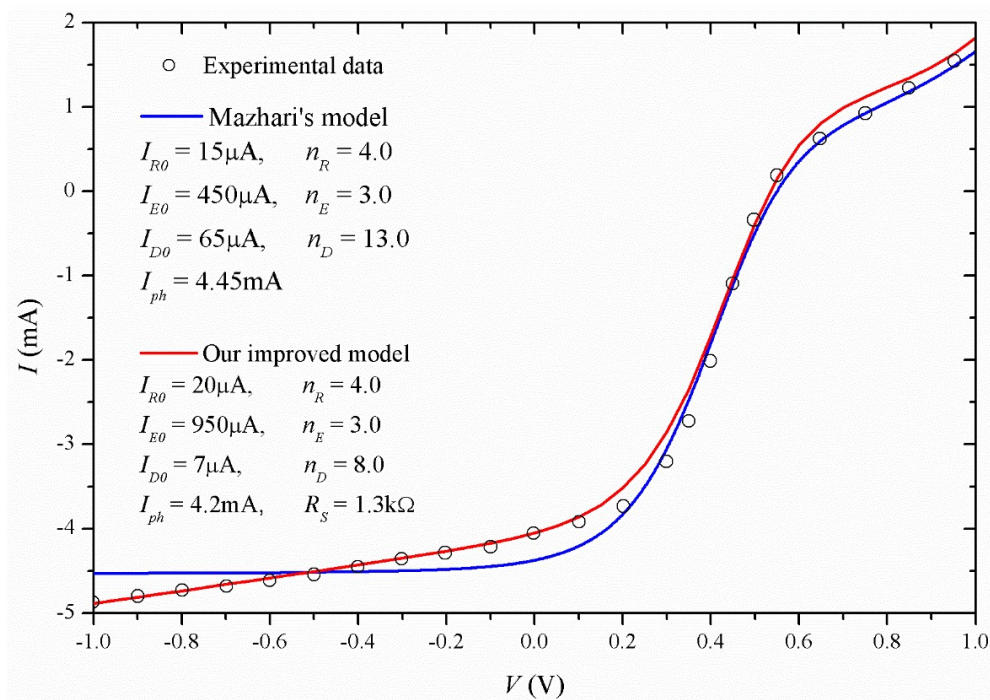**Figure 9.** Comparisons between our solutions of Mazhari's model and the experimental data [19] without annealing.



**Figure 10.** Comparisons between our solutions of Mazhari's model and the experimental data [19] with annealing at 120 °C.
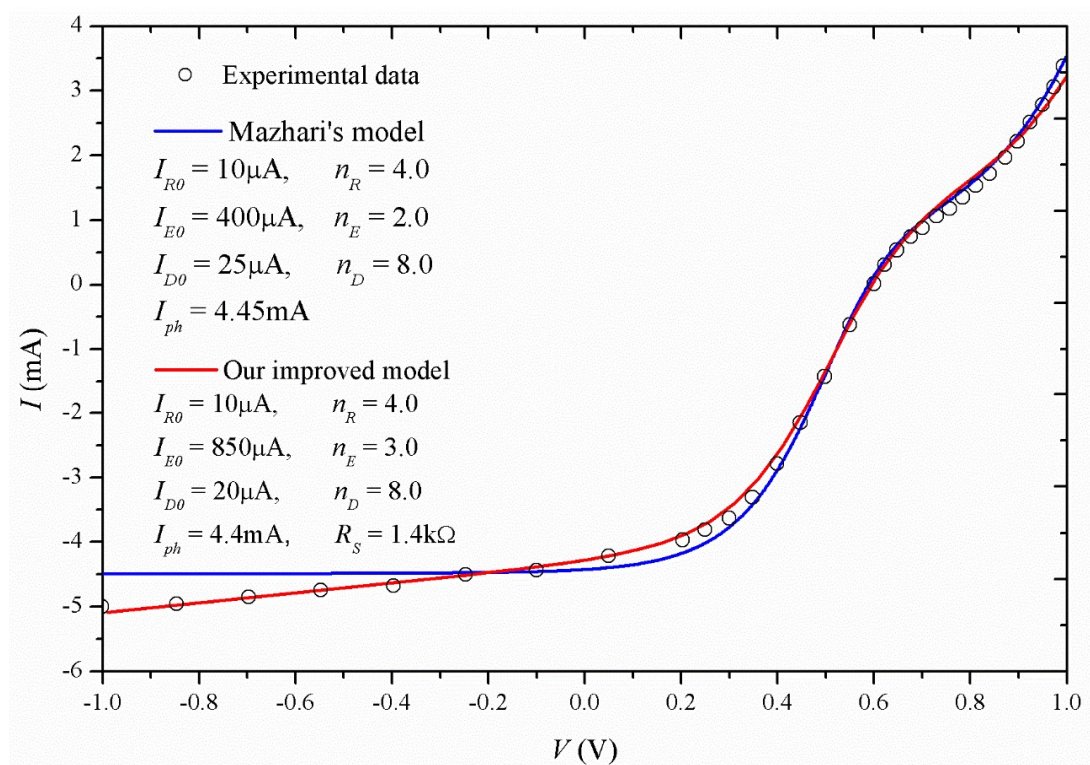
**Figure 11.** Comparisons between our solutions of Mazhari's model and the experimental data [19] with annealing at 150 °C.
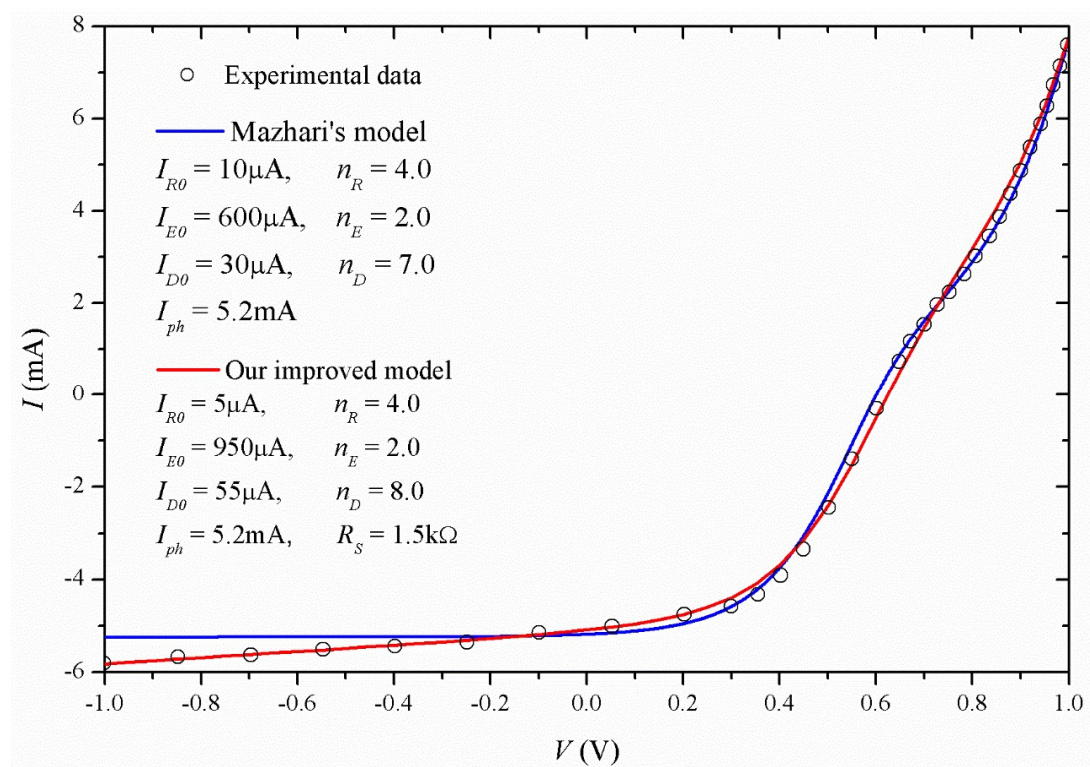


**Figure 12.** Comparisons between our solutions of Mazhari's model and the experimental data [19] with annealing at 180 °C.
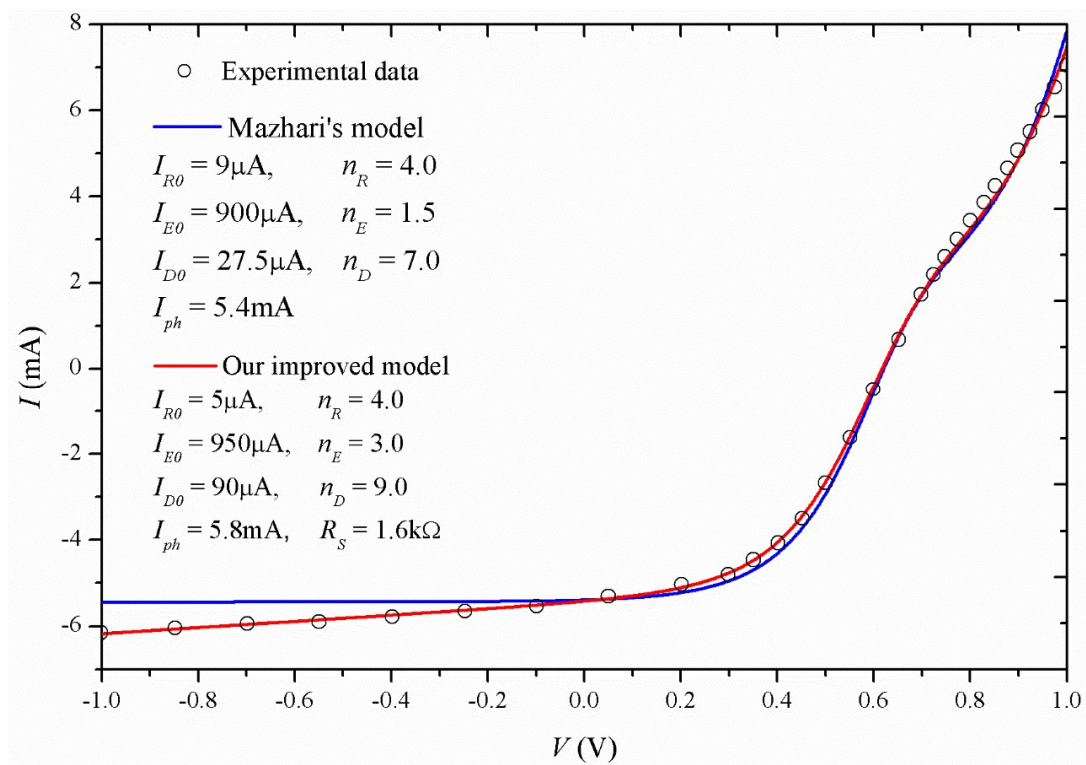
**Figure 13.** Comparisons between our solutions of Mazhari's model and the experimental data [19] with annealing at 200 °C.

For the solar cells in Reference [19], the enhanced electron acceptor (fullerene C60) and donor (purified Poly[2-methoxy-5-(2-ethylhexyloxy)-1,4-phenylene-vinylene]) bilayer films were prepared on clean ITO glass coated with 50 nm of PEDOT:PSS and 50 nm of Al cathode, with the aim of increasing the power conversion efficiency (PCE). In the $N_2$ atmosphere, the solar cells in [19] were exposed to 1000 W/m$^2$ simulated AM1.5G sunlight, and the *I–V* characteristics were measured and shown as symbols in Figures 9–13.

According to Figures 9–13, and combining the equation set of (1) and (2), we can observe that our improved model can simulate the S-shaped kink with both the exponent-like rise in the first quadrant and the linear-like rise in the third quadrant. From the view of physical significance, the shunt resistance should be added to the loss of the current. From the view of circuit structure, our improved model can degrade into Mazhari's model under the condition that $R_S$ goes into infinity. From the view of simulation results, we can observe that our improved model can give more accurate predictions on the linear-like rise of the S-shaped kink in the third quadrant, compared with Mazhari's model. This is the reason why the shunt resistance $R_S$ must be introduced in our improved model. It is interesting that the slope of the S-shaped kink in the third quadrant decreases, but the shunt resistance $R_S$ increases as the annealing temperature increases. The probable reason is that the increase of annealing temperature results in the increase of contact resistance $R_s$. In addition, the higher annealing temperature leads to the *I–V* curves of OSCs changing from S-shape into J-shape. This may result from the mixture of donor and acceptor.

## 5. Conclusions

In this paper, we proposed an improved model based on Mazhari's model and derived the analytical solution of our improved model by using the Newton-Raphson root-finding scheme. High accuracy and efficiency of solutions show that our improved model, as a lumped-parameter equivalent circuit model, can be used to simulate the S-shaped *I–V* characteristics of organic solar cells (OSCs).

Compared with Mazhari's model, the simulation results of our improved model for S-shaped kink are more accurate in the third quadrant. Finally, we used the least square method and experimental data to verify our solutions of the improved model. As a result, such an improved model can be adopted to substitute for Mazhari's model to give more accurate predictions on the S-shaped *I–V* characteristics of OSCs, especially for the S-shaped kink in the third quadrant.

**Author Contributions:** C.X. and F.Y. conceived and wrote the paper and designed and performed the simulations; G.H. and W.L. finally analyzed the data; C.X. contributed to analysis tools.

**Conflicts of Interest:** The authors declare no conflicts of interest.

## References

1. Wagenpfahl, A.; Rauh, D.; Binder, M.; Deibel, C.; Dyakonov, V. S-shaped current-voltage characteristics of organic solar devices. *Phys. Rev. B* **2010**, *82*, 115306. [CrossRef]
2. Tran, V.H.; Ambade, R.B.; Ambade, S.B.; Lee, S.H.; Lee, I.H. Low-temperature solution-processed SnO$_2$ nanoparticles as cathode buffer layer for inverted organic solar cells. *ACS Appl. Mater. Interfaces* **2017**, *9*, 1645–1653. [CrossRef] [PubMed]
3. Kim, T.; Kim, J.-H.; Kang, T.E.; Lee, C.; Shin, M.; Wang, C.; Ma, B.; Jeong, U.; Kim, T.-S.; Kim, B. Flexible, highly efficient all-polymer solar cells. *Nat. Commun.* **2015**, *6*, 8547. [CrossRef] [PubMed]
4. He, Z.; Zhong, C.; Su, S.; Xu, M.; Wu, H.; Cao, Y. Enhanced power-conversion efficiency in polymer solar cells using an inverted device structure. *Nat. Photonics* **2012**, *6*, 591–595. [CrossRef]
5. Liu, Y.; Zhao, J.; Li, Z.; Mu, C.; Ma, W.; Hu, H.; Jiang, K.; Lin, H.; Ade, H.; Yan, H. Aggregation and morphology control enables multiple cases of high-efficiency polymer solar cells. *Nat. Commun.* **2014**, *5*, 5293. [CrossRef] [PubMed]
6. Chavali, R.V.K.; Li, J.V.; Battaglia, C.; Wolf, S.; Gray, J.L.; Alam, M.A. A generalized theory explains the anomalous Suns–*Voc* response of Si heterojunction solar cells. *IEEE J. Photovolt.* **2017**, *7*, 169–176. [CrossRef]
7. Yoshikawa, K.; Kawasaki, H.; Yoshida, W.; Irie, T.; Konishi, K.; Nakano, K.; Uto, T.; Adachi, D.; Kanematsu, M.; Uzu, H. Silicon heterojunction solar cell with interdigitated back contacts for a photo conversion efficiency over 26%. *Nat. Energy* **2017**, *2*, 17032. [CrossRef]
8. Castro, F.A.; Heier, J.; Nuesch, F.; Hany, R. Origin of the kink in current-density versus voltage curves and efficiency enhancement of polymer-C60 heterojunction solar cells. *IEEE J. Sel. Top. Quantum Electron.* **2010**, *16*, 1690–1699. [CrossRef]
9. Jain, A.; Kapoor, A. A new approach to study organic solar cell using Lambert W-function. *Sol. Energy Mater. Sol. Cells* **2005**, *86*, 197–205. [CrossRef]
10. Cheknane, A.; Hilal, H.S.; Djeffal, F.; Benyounce, B.; Charles, J.-P. An equivalent circuit approach to organic solar cell modelling. *Microelectron. J.* **2008**, *39*, 1173–1180. [CrossRef]
11. Mazhari, B. An improved solar cell circuit model for organic solar cells. *Sol. Energy Mater. Sol. Cells* **2006**, *90*, 1021–1033. [CrossRef]
12. Kumar, P.; Gaur, A. Model for the *J-V* characteristics of degraded polymer solar cells. *J. Appl. Phys.* **2013**, *113*, 094505. [CrossRef]
13. García-Sánchez, F.J.; Lugo-Muñoz, D.; Muci, J.; Ortiz-Conde, A. Lumped parameter modeling of organic solar cells' S-shaped *I-V* characteristics. *IEEE J. Photovolt.* **2013**, *3*, 330–335. [CrossRef]
14. Zuo, L.; Yao, J.; Li, H.; Chen, H. Assessing the origin of the S-shaped *I-V* curve in organic solar cells: An improved equivalent circuit model. *Sol. Energy Mater. Sol. Cells* **2014**, *122*, 88–93. [CrossRef]
15. Castro, F.A.; Heier, J.; Nuesch, F.; Hany, R. Origin of the kink in current-density versus voltage curves and efficiency enhancement of polymer-C60 heterojunction solar cells. *IEEE J. Sel. Top. Quantum Electron.* **2010**, *16*, 1690–1699. [CrossRef]
16. Roland, P.J.; Bhandari, K.P.; Ellingson, R.J. Electronic Circuit Model for Evaluating S-Kink Distorted Current-Voltage Curves. In Proceedings of the Photovoltaic Specialists Conference (PVSC), Portland, OR, USA, 5–10 June 2016; IEEE: Piscataway, NJ, USA, 2016; pp. 3091–3094.

17. Laudani, A.; Fulginei, F.R.; De Castro, F.; Salvini, A. Irradiance intensity dependence of the lumped parameters of the three diodes model for organic solar cells. *Sol. Energy* **2018**, *163*, 526–536. [CrossRef]
18. Romero, B.; Pozo, G.; Arredondo, B.; Martín-Martín, D.; Gordoa, M.P.R.; Pickering, A.; Pérez-Rodríguez, A.; Barrena, E.; García-Sánchez, F.J. S-shaped *I-V* characteristics of organic solar cells: Solving Mazhari's lumped-parameter equivalent circuit model. *IEEE Trans. Electron Devices* **2017**, *64*, 4622–4627. [CrossRef]
19. Huang, G.; Yu, F.; Xu, C. An Analytical Solution to Lumped Parameter Equivalent Circuit Model of Organic Solar Cells. *Crystals* **2018**, *8*, 224. [CrossRef]
20. Castro, F.A.; Laudani, A.; Fulginei, F.R.; Salvini, A. An in-depth analysis of the modelling of organic solar cells using multiple-diode circuits. *Sol. Energy* **2016**, *135*, 590–597. [CrossRef]
21. Shockley, W. The theory of p-n junctions in semiconductors and p-n junction transistors. *Bell Syst. Tech. J.* **1949**, *28*, 435–489. [CrossRef]